Protocol for pulsed antihydrogen production in the AE$\bar{g}$IS apparatus

I C Tietje,[1,2] C Amsler,[3] M Antonello,[4,5] A Belov,[6] G Bonomi,[7,8] R S Brusa,[9,10] M Caccia,[4,5] A Camper,[1] R Caravita,[10] F Castelli,[5,11] P Cheinet,[12] D Comparat,[12] G Consolati,[5,13] A Demetrio,[14] L Di Noto,[15,16] M Doser,[1] M Fanì ,[1,15,16] R Ferragut,[5,17] J Fesel,[1] S Gerber,[1] M Giammarchi,[5] A Gligorova,[3] L T Glöggler,[1] F Guatieri,[9,10] S Haider,[1] A Hinterberger,[1] A Kellerbauer,[18] O Khalidova,[1] D Krasnický ,[16] V Lagomarsino,[16] C Malbrunot,[1] L Nowak,[1] S Mariazzi,[9,10] V Matveev,[6] S R Müller,[14] G Nebbia,[19] P Nedelec,[20] M Oberthaler,[14] E Oswald,[1] D Pagano,[7,8] L Penasa,[9,10] V Petracek,[21] L Povolo,[9,10] F Prelz,[5] M Prevedelli,[22] B Rienäcker,[1] O M Røhne,[23] A Rotondi,[8,24] H Sandaker,[23] R Santoro,[4,5] G Testera,[16] V Toso,[5,17] T Wolz,[1] P Yzombard,[18] C Zimmer,[1,23,25] and N Zurlo[8,26]

[1] Physics Department, CERN, 1211 Geneva 23, Switzerland
[2] Centre of Astronomy and Astrophysics, TU Berlin, 10623 Berlin, Hardenbergstraße 36, D-10623 Berlin, Germany
[3] Stefan Meyer Institute for Subatomic Physics, Austrian Academy of Sciences, Boltzmanngasse 3, 1090 Vienna, Austria
[4] Department of Science, University of Insubria, Via Valleggio 11, 22100 Como, Italy
[5] INFN Milano, via Celoria 16, 20133 Milano, Italy
[6] Institute for Nuclear Research of the Russian Academy of Science, Moscow 117312, Russia
[7] Department of Mechanical and Industrial Engineering, University of Brescia, via Branze 38, 25123 Brescia, Italy
[8] INFN Pavia, via Bassi 6, 27100 Pavia, Italy
[9] Department of Physics, University of Trento, via Sommarive 14, 38123 Povo, Trento, Italy
[10] TIFPA/INFN Trento, via Sommarive 14, 38123 Povo, Trento, Italy
[11] Department of Physics "Aldo Pontremoli", University of Milano, via Celoria 16, 20133 Milano, Italy
[12] Laboratoire Aimé Cotton, Université Paris-Sud, ENS Paris Saclay, CNRS, Université Paris-Saclay, 91405 Orsay Cedex, France
[13] Department of Aerospace Science and Technology, Politecnico di Milano, via La Masa 34, 20156 Milano, Italy
[14] Kirchhoff Institute for Physics, Heidelberg University, Im Neuenheimer Feld 227, 69120 Heidelberg, Germany
[15] Department of Physics, University of Genova, via Dodecaneso 33, 16146 Genova, Italy
[16] INFN Genova, via Dodecaneso 33, 16146 Genova, Italy
[17] LNESS, Department of Physics, Politecnico di Milano, via Anzani 42, 22100 Como, Italy
[18] Max Planck Institute for Nuclear Physics, Saupfercheckweg 1, 69117 Heidelberg, Germany
[19] INFN Padova, via Marzolo 8, 35131 Padova, Italy
[20] Univ Lyon, Univ Claude Bernard Lyon 1, CNRS/IN2P3, IP2I Lyon, F-69622, Villeurbanne, France
[21] Czech Technical University, Prague, Brehov 7, 11519 Prague 1, Czech Republic
[22] University of Bologna, Viale Berti Pichat 6/2, 40126 Bologna, Italy
[23] Department of Physics, University of Oslo, Sem Slandsvei 24, 0371 Oslo, Norway

[24] Department of Physics, University of Pavia, via Bassi 6, 27100 Pavia, Italy
[25] Department of Physics, Heidelberg University, Im Neuenheimer Feld 226, 69120 Heidelberg, Germany
[26] Department of Civil, Environmental, Architectural Engineering and Mathematics, University of Brescia, via Branze 43, 25123 Brescia, Italy

E-mail: ingmari.tietje@cern.ch

Abstract. The AE$\bar{g}$IS collaboration's main goal is to measure the acceleration of antihydrogen ($\bar{H}$) due to gravity. The experimental scheme is to form a pulsed beam whose vertical deflection is then measured by means of a moiré deflectometer [1]. Creating pulsed $\bar{H}$ is crucial since it allows a velocity measurement of the antiatoms via time of flight (ToF) necessary to deduce the gravitational acceleration $\bar{g}$ from the vertical deflection Δs. The aim of this article is to outline the experimental protocol leading up to pulsed antihydrogen production in the AE$\bar{g}$IS experiment.

1. Introduction

The matter antimatter imbalance in the visible part of our universe has been cause for an abundance of hypotheses [2, 3, 4, 5], of which some assume a breaking of the WEP (weak equivalence principle) or CPT (Charge, Parity and Time reversal) symmetry [6]. The WEP is one of the pillars of the theory of General Relativity (GR) and the Standard Model (SM) of particle physics relies on CPT symmetry. The search for a discrepancy between the behaviour of antimatter toward matter in a gravitational field and e.g. the energy level structure between an antiatom and an atom therefore serves as a test of GR and SM, respectively.

To help resolve speculations as to the cause of the baryon asymmetry, experiments try and shed more light on the open questions of whether the WEP and/or CPT symmetry experience violations [7, 8, 9].

In the low-energy antimatter collaborations based at CERN (Conseil Européen pour la Recherche Nucléaire) the lightest stable antiatom – antihydrogen ($\bar{H}$) – is at the heart of many experiments probing for (minimal) violations of the WEP and CPT symmetry.

Among the experiments testing for WEP [10, 11] is the AE$\bar{g}$IS collaboration with the experimental pursuit of probing how antihydrogen 'falls' in the gravitational field of Earth.

AE$\bar{g}$IS experimental scheme [1] relies on the generation of a pulsed antihydrogen beam that traverses a gravity module [12, 13] which is designed to measure the vertical deflection of the anti-atoms. The pulsed nature of the beam allows a velocity measurement through ToF which is necessary to determine the deflection Δs due to gravity over a horizontal distance d.

While the concept of this measurement is straightforward, the experimental implementation is rather complex since we live in a matter universe where antimatter is scarce. In AE$\bar{g}$IS, experimental techniques from non-neutral plasma (NNP) [14], positron (e^+), [15], positronium[1] (Ps) [16], laser and detector physics [13] are orchestrated. Non-neutral plasma physics is employed for the trapping of antiprotons ($\bar{p}$) and their manipulation via electrons confined in the same trap. Positrons are accumulated, buffer-gas-cooled and stored in Penning/Penning-Malmberg traps [17]. Positronium and laser physics go hand in hand: positronium is generated

[1] The instable 'quasi'-atom exhibits an energy structure at half the binding energy of that of hydrogen $E_0 = 13.6\text{eV} \cdot \mu/m_{e^-} = -6.8\text{eV}$ with the reduced mass of $\mu = m_{e^-}/2$. Electron and positron orbit about their centre of mass and occupy roughly the same volume as hydrogen. Positronium has two possible ground states: the triplet state $s = 1$ ($\uparrow\uparrow$, $\downarrow\downarrow$, $(\uparrow\downarrow + \downarrow\uparrow)/\sqrt{2}$) and the singlet state ($(\uparrow\downarrow - \downarrow\uparrow)/\sqrt{2}$) refered to as ortho- and para-Ps, repectively. While para-Ps decays into 2γ photons, ortho-Ps decays into 3γ photons with a combined energy of 1022keV.

by injecting a bunch of positrons into a nanochannelled silicon target [18]. The lifetime of ortho-Ps is increased by several orders of magnitude with respect to the ground state, by a two-step excitation into a desired Rydberg state. Arranging these experimental techniques in a suitable way makes for an experimental protocol leading up to pulsed antihydrogen generation.

In Section 2 we will illustrate the experimental scheme employed in AE$\bar{g}$IS leading up to pulsed antihydrogen production. In Section 2.1, we will give a brief description of the scintillating detectors used for antiproton monitoring and which are also suitable for antihydrogen detection. Sections 2.2 and 2.3 detail the simultaneous preparation of antiprotons and positrons, while Sections 2.4 and 2.5 shed light on the pulsed positronium generation and excitation, respectively. The focus of Section 2.6 is the orchestration of all previous Sections – in other words – pulsed antihydrogen generation. Sections 3 and 4 summarise, discuss and give a perspective on possible future endeavours of the AE$\bar{g}$IS collaboration.

2. Experimental Scheme

For the formation of antihydrogen through charge-exchange antiprotons and positrons are prepared simultaneously, see Fig. 1.

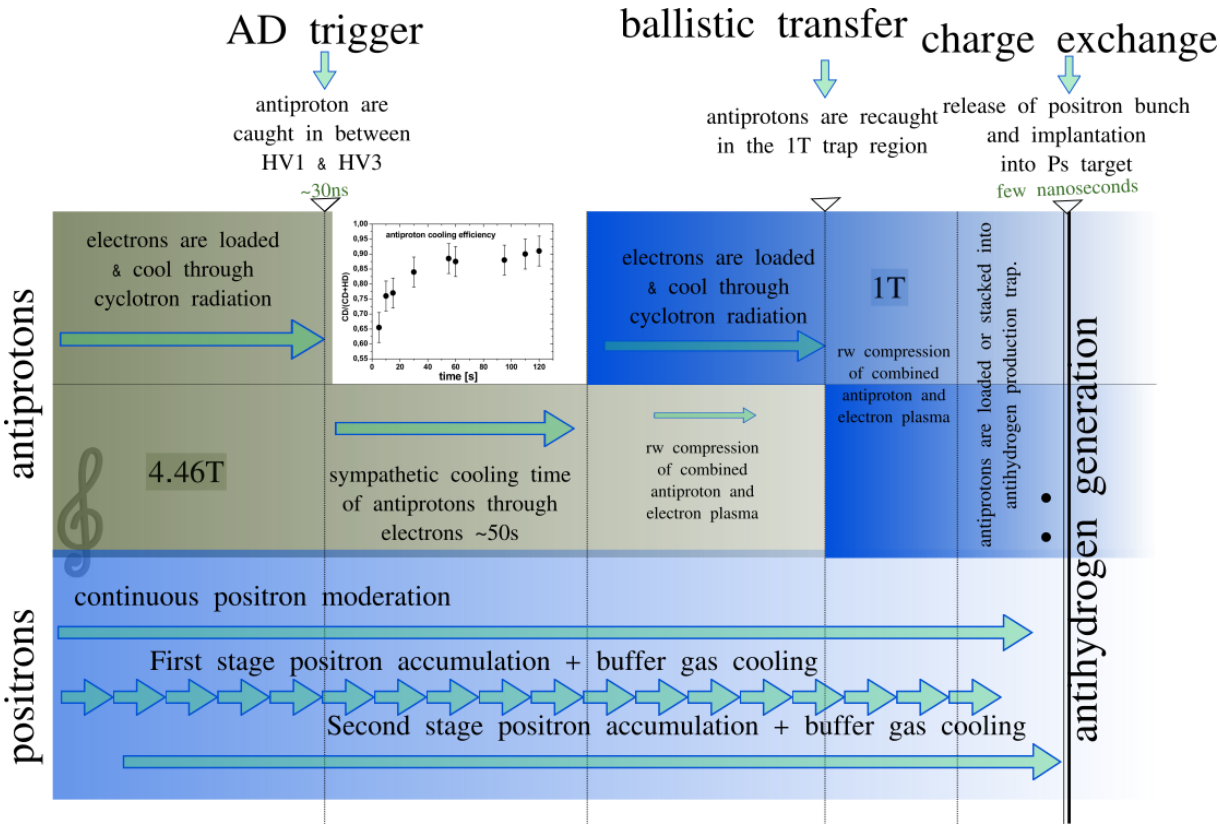

Figure 1. Experimental protocol leading up to antihydrogen production.

The antiprotons are provided by the CERN infrastructure [19]. Antiproton bunches are injected into the AE$\bar{g}$IS experiment beam line at an energy of 5 MeV. By passage through a combined silica-aluminium target they loose a great fraction of their kinetic energy, scatter or annihilate. The decelerated antiprotons with an energy of less than 9 keV are trapped in the magnetic and electric fields of the catching region of the AE$\bar{g}$IS main apparatus, see Fig. 2.

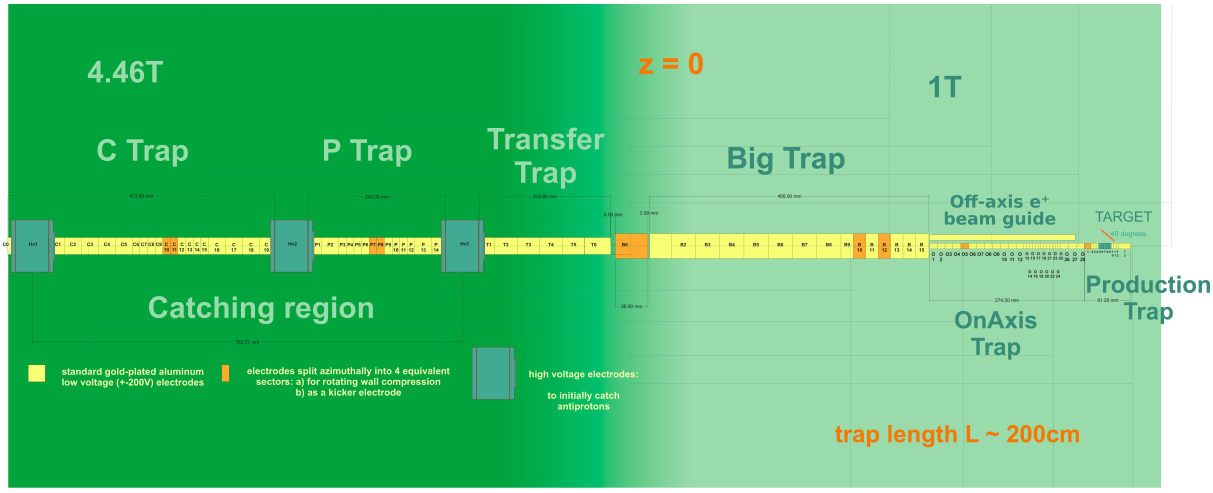

Figure 2. The main trap assembly contains a stack of ~ 190 electrodes placed in the evacuated and cryogenic core of two superconducting solenoid magnets that give rise to a homogeneous magnetic field. The Ctrap and Ptrap which are located in the 4.46 T region are used for loading electrons (Ctrap) as well as the manipulation/preparation of electron and combined electron-antiproton plasmas (Ptrap). The transfer trap bridges the crossing from the high-field 4.46 T catching region to the 1 T antihydrogen production region. The Big Trap, the OnAxis Trap and the antihydrogen production trap are located in the 1 T field. The Big Trap is important for loading electrons into the production trap while the OnAxis trap can be used for plasma oscillation studies. Positrons are injected into the positronium target located above the antihydrogen production trap through the e^+ beam guide. The production trap is designed for the purpose of pulsed antihydrogen production, cf. Fig. 4. The higher field of 4.46 T is beneficial for catching and manipulating antiprotons while the lower 1 T field prevents significant quenching and thereby loss of either Rydberg positronium or antihydrogen.

The confined antiprotons are cooled down via electron-cooling to the environment's cryogenic temperatures, compressed and ballistically transfered into the antihydrogen production trap. In this trap the charged particles are recooled with newly loaded electrons, stored and also stacked.

Within the same time span, moderated positrons are accumulated from a radioactive source, buffer-gas-cooled, accumulated and stored in a Surko type trap assembly. A positron bunch is released from the trap assembly and guided into the main apparatus positronium conversion target, see Fig. 2, through a 45 degree transfer line, see Fig. 3.

The 4.6 keV e^+ bunch is injected into the nanochannelled target which is located in close proximity above the antihydrogen production trap, see Fig. 4. The generated positronium, exiting from the target, is brought into a Rydberg state via a two-step laser excitation (UV and IR), see Section 2.5.

Through the perforated mesh of the antihydrogen production trap electrodes, cf. Fig. 4, Rydberg positronium can enter and undergo charge exchange with the stored antiprotons

$$\bar{p} + Ps^* \rightarrow \bar{H} + e^- \ . \tag{1}$$

Antihydrogen is neutral and thus once it is generated travels freely until it annihilates on the trap wall, the signal of which is registered by a scintillating detector.

The objective is to Stark accelerate pulsed antihydrogen to create a pulsed $\bar{H}$ beam. A gravity module will admit the beam and detect the deflection of antihydrogen due to free fall.

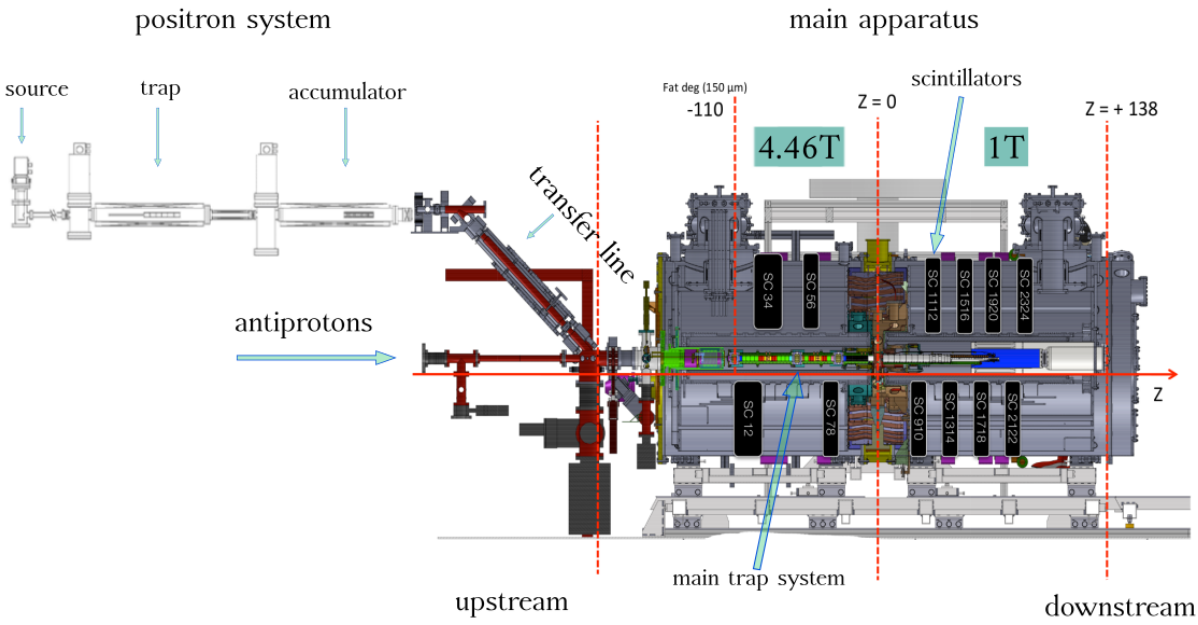

Figure 3. The AE$\bar{g}$IS apparatus consists of the main trap assembly, the positron system, the laser system as well as a set of detectors. The positron system is mounted upstream from the main trap system. It is comprised of a Na^{22} source with moderator, two adjacent Surko-type traps called 'trap' and 'accumulator' and connected to the main trap system via a transfer line at 45 degree. As indicated antiproton bunches enter from upstream and are caught in the 4.46 T part of the main trap system. The 1 T part further downstream is the designated area for pulsed antihydrogen production. While the positron system is operated at room temperature the main trap system offers cryogenic temperatures. For simplicity, we omitted the laser system, which is located close to the 4.46 T magnet. Its UV and IR laser light reaches the interaction region close to the positronium target in the 1 T region of the main traps via a viewport and an optical system which is located inside the main vessel.

While Stark acceleration has not been performed yet, the gravity module was successfully tested with antiprotons [12].

This article focusses on the experimental scheme leading up to pulsed antihydrogen generation in the AE$\bar{g}$IS apparatus. The reader may refer to the relevant literature for Stark acceleration and gravity module [12, 20].

Before we elucidate the details of the experimental procedure we will give a brief survey of the scintillating detectors.

2.1. Scintillating detectors

Fig. 3 depicts 12 external scintillators which are arranged around the main apparatus. A 1 cm thick scintillator slab that arches over 1/3 of a full circle, i.e. 120 degrees, is placed either above of below the magnets, respectively. Each end of a slab is read out by a PMT (photo multiplier tube) totalling 2 PMTs per slab.

The PMTs register the signals steming from the scintillator arc once a particle traverses the slab. The recorded signal relates proportionally to the number of annihilated antiprotons, where each antiproton annihilation gives rise to an average of $2-3$ charged pions [13, 21].

There are two modes of operation: the continuous operation mode, in principle, allows for a maximal saturation limit of 20 MHz or a discrimation of 50 ns between two events, respectively.

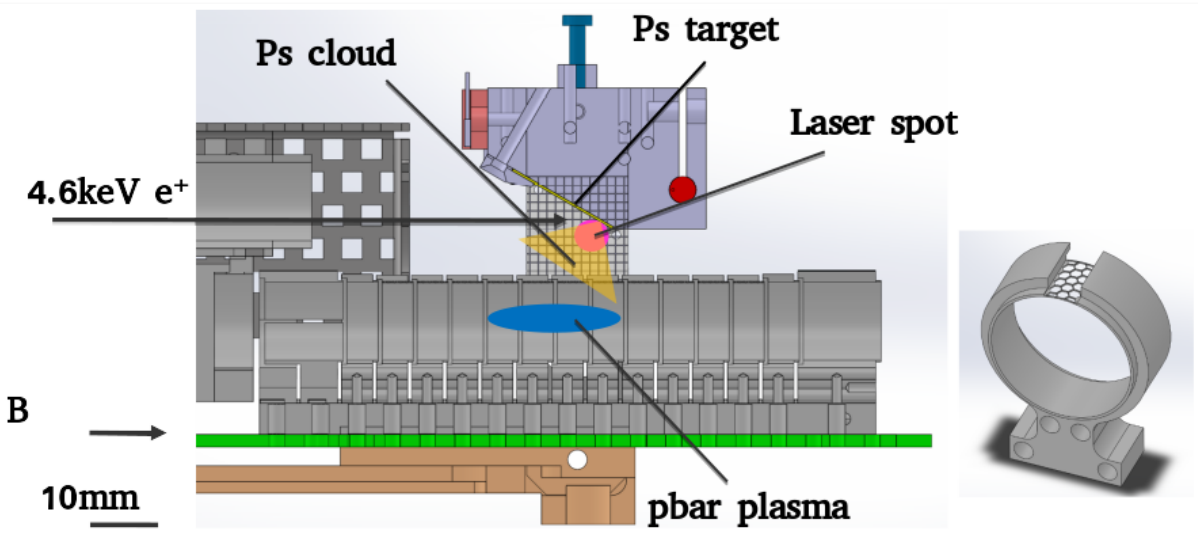

Figure 4. The heart of the experiment is comprised of the antihydrogen production trap and the positronium target which is mounted above the partially perforated trap electrodes. When a positron bunch is injected into the target it traverses a biased off-axis e^+ beam guide. Generated Ps is emitted into 2π (precise steradian), excited into a Rydberg state via a two-step laser excitation (UV + IR) and a fraction of Ps* travels through the perforated top parts of the relevant production trap electrodes. When a Ps* comes close to one of the stored antiprotons, the 'quasi'-atom and the antiparticle can undergo charge-exchange and form Rydberg antihydrogen while setting an electron free (Eq. (1)).

The maximal measurable detection rate taking into account signal rise and fall times as well as jitters corresponds to 15 MHz, i.e. 1.5 events in 100 ns.

An alternative mode of operation is to record the analogue PMT signal outputs by means of a digitiser spanning a time window of about 5 ms. The analogue variation of the signal is recorded via a V1720 Flash ADC Waveform Digitiser with a time resolution of 4 ns (250 MS/s) and an amplitude resolution of 0.5 mV (12 bit for a dynamic input range of 2 Vpp). The scintillator slabs closer to the antihydrogen production trap can be used to measure the production rate of antihydrogen. For in-depth reading on the scintillator slabs we refer the reader to ref. [22].

2.2. Antiproton catching, cooling and manipulation

The antiproton beam's injection energy into the AE$\bar{g}$IS beam line of 5 MeV exceeds the energies of particles to be caught in the cryogenic main trap assembly Penning Malmberg traps, see Fig. 2. A degrader foil of $\sim 225\,\mu$m thickness Aluminium equivalent is used to decelerate the antiprotons to a trappable energy regime of the order of 10 keV. In the process most antiprotons are lost due to the scattering and annihilations within the degrader. Solely 1 % of the impinging antiprotons are caught and trapped within the 4.46 T catching region of the main trap system owing to the losses due to degrader and limited trapping voltages of 9 kV applicable to the high voltage electrodes HV1, HV2 and HV3.

After the passage through the degrader the charged particle bunch is deflected by the steep field of high-voltage electrode HV3, which is biased to 9 kV. During a few tens of nanoseconds, and with a delay of $600 - 800$ ns (timed with respect to when the antiprotons first enter the AE$\bar{g}$IS main apparatus), the voltage bias on electode HV1 is raised to 9 kV and up to 500 000 antiprotons are trapped.

The $\bar{p}$s repeatedly make turns through the preloaded electron plasma which is in thermal equilibrium with the cryogenic environment. The antiprotons, which are too heavy to cool through their own cyclotron motion are cooled to environmental cryogenic temperatures via collisions with the electrons.

After sufficient cooling the high voltage electrodes HV1 and HV3 are switched off. For a cooling duration of 50 s a fraction of 60 % of initially trapped antiprotons are cold enough as to remain in the low-voltage trap in the Ptrap region, see Fig. 2, that confines the cryogenic electrons. The 'hot' fraction of antiprotons is lost and its annihilation signal is recorded via the scintillators in continuous operation, cf. Section 2.1.

Subsequently, the two-component antiproton-electron plasma is prepared for transfer into the antihydrogen production trap, see Fig. 4. During the ballistic transfer to the downstream $\bar{H}$ production region the two-component plasma inflates radially by a factor of $\sqrt{4.46\,T/1\,T} = 2.1$. It is crucial to compress the plasma before its inflation by means of the 'rotating wall' (rw) technique [23] to prevent $\bar{p}$ losses on the trap walls in the 1 T magnet: the plasma rotation frequency is increased which for non-neutral plasmas (in thermal equilibrium) confined in Penning or Penning-Malmberg traps is tantamount to a compression of the plasma radius [14, 24].

In the process of the ballistic transfer the electrons are lost. Electrons are newly loaded and trapped in the 1T field before the $\bar{p}$ transfer and precool through cyclotron radiation in the OnAxis trap, see Fig. 2. From the OnAxis trap, see Fig. 2, the two-species plasma is shifted adiabatically to the antihydrogen production trap where it is stored underneath the partially perforated electrodes, see Fig. 4.

The experimental protocol is repeated and antiprotons are stacked in the antihydrogen production trap, whereby we have achieved an up-to 3-fold increase in particle number available for pulsed charge-exchange (Eq. (1)).

2.3. Positron moderation, accumulation, cooling and preparation

AE$\bar{g}$IS obtains the positrons that are used in the experimental sequence from a radioactive ^{22}Na source (1.5 GBq in January 2016). To provide the positrons in form of a pulsed beam the particles have to be moderated and directed, collected, cooled and accumulated, all of which will be examined in the following. A repeated release from the Surko type trap assembly ensures a pulsed positron beam.

2.3.1. Positron moderation: the ^{22}Na source's broad e^+ energy spectrum and its 4π emittance are moderated and directed via a conically shaped moderator [25]. Behind the source sits a Titanium block that reflects some of the backward emitted positrons into the cone.

The geometry of the copper cone on which the solid neon moderator (with positive work function [26]) is grown at 7 K, permits multiple passages through the moderator causing the e^+ to rapidly loose their kinetic energy [27] while favouring an ejection parallel to the cone's symmetry axis.

The positive work function of Neon enhances the chance that the e^+ overcome the solid to vacuum surface barrier. The yield of positrons is enhanced by biasing the source head to 18 V which helps to expell particles from the source. The efficiency ϵ in such a configuration ($\epsilon = 7\times10^{-3}$ [28]) is anticipated to exceed the moderation for tungsten ($\epsilon = 1.2\times10^{-3}$ [29]). The higher efficiency facilitates the choice of a neon moderator, which is dependent on cryogenics, over tungsten meshes or foils that can be operated at room temperature [30].

The flux of positrons exits the moderator in the form of a continuous and monochromatic beam of well-defined energy.

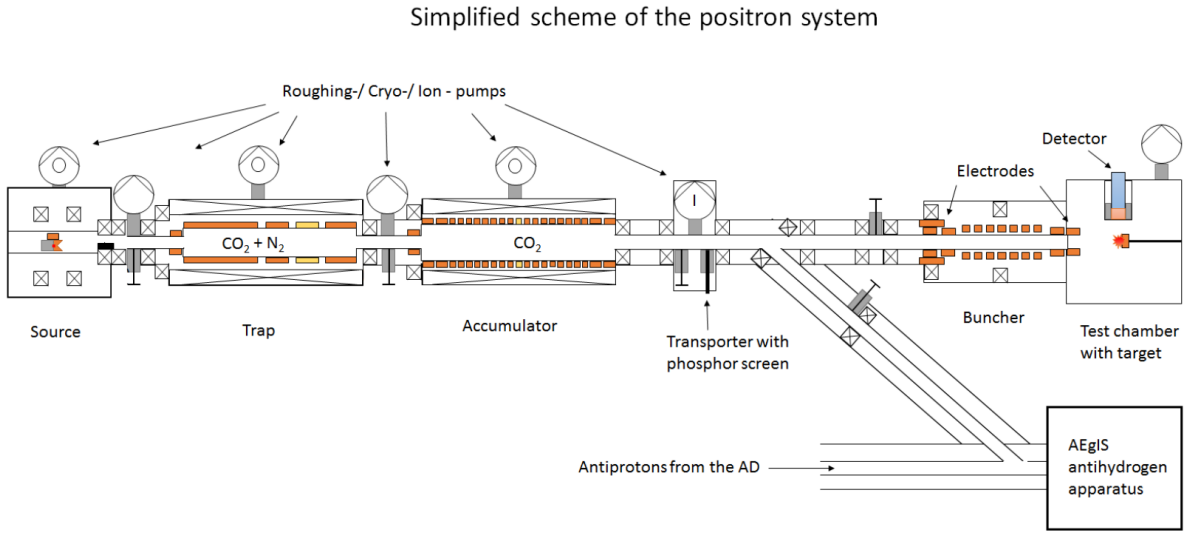

Figure 5. Overview of the AE$\bar{g}$IS positron system.

2.3.2. Buffer-gas cooling and accumulation of positrons: from the source, see Fig. (5), the positrons are magnetically guided into a Surko type trap assembly [31] consisting of the so-called 'trap' and 'accumulator', which are both Penning-Malmberg type traps which are filled with buffer-gas. The principle in both traps is that the e^+ has enough kinetic energy to enter but refrains from exiting the trap potential due to rapid buffer-gas cooling [31]. The efficiency of cooling the antiparticles competes with loss of positrons through the annihilation channel. A higher buffer-gas pressure in the 'trap', see Fig. 5, provides a rapid cooling channel via buffer-gas species CO_2 and N_2. Positrons are accumulated in the 'trap' for 150 ms and then stored for 2 ms. At a rate of 6.5 Hz small positron bunches from the 'trap' are released toward and stacked in the 'accumulator'. Higher numbers of positrons can be cooled, stored and stacked with a less prevailing annihilation channel owing to the lower buffer-gas pressure (10^{-8}mbar CO_2) at 100mT radially confining field.

An accumulation of 1000 pulses released from the 'trap' provides around 1.1×10^7 positrons. A harmonic axial trap shape in the accumulator decreases the axial positron plasma length as the particles cool and gives rise to a sharper bunch shape once released and transfered.

2.3.3. Release and transfer: a potential ramp accelerates the positron bunch to 300 eV (energy necessary to prevent magnetic reflection upon entering the much higher magnetic fields in the main apparatus). The correct passage into the 45 degree transfer line, see Fig. 3, is guaranteed by an angled solenoid. In the transfer line the e^+ bunch is accelerated to 4.6 keV. Once in the main trap system the trajectory of the antiparticles is determined by the magnetic field lines in the 4.46 T and 1 T regions. Several diagnostics are present in the beam path (among them a phosphor screen which is insertable into the beam path and a MCP in the 1 T region) which help the correct implantation of the particles into the nanochannelled silicon positronium target. Practically no expansion of the bunch happens before its implantation into the positronium target.

2.4. Pulsed positronium generation

The generation of positronium in the AE$\bar{g}$IS apparatus takes place via the injection of a 4.6 keV positron bunch into a nanochannelled silicon target [18] refered to as the positronium target.

The positrons loose their kinetic energy in the bulk of the target material and a fraction reaches the surface of the nanochannels which is comprised of native silica, and where chances are high a positron forms positronium with a material electron.

Due to its transience para-Ps annihilates close to where it was generated, i.e. inside the positronium target. The longevity of ortho-Ps permits multiple reflections of the 'quasi'-atom inside the nanochannels that permeate the target. The contact with the channel walls of the cold target serves as partial moderation.

The Ps exiting the target need to be sufficiently long-lived to cover the distance from the target through the perforated antihydrogen production trap sections to reach the antiprotons stored in the trap and undergo charge exchange. The life-time of Ps increases with the cube of its principle quantum number

$$\tau \propto n^3 \ . \tag{2}$$

Since the cross section for the charge-exchange reaction increases with n^4 laser excitation seems the obvious choice.

2.5. Laser physics and positronium preparation

The Ps is brought into a Rydberg state via a two-state excitation from $n = 0 \rightarrow n = 3$ and $n = 3 \rightarrow$ Rydberg state. The laser system that provides the pulses is comprised of a Q-switched Nd:Yag laser combined with an OPG (optical parametric generator) and OPA (optical parametric amplifier).

The 1.5 ns UV pulse with 118 GHz bandwidth has an energy of 80 μJ and it is produced from the second and fourth harmonic of the laser. It is tuneable from 204.9 nm to 205.2 nm. The 3 ns IR pulse has a bandwidth of 430 GHz at 1.5 mJ, driving the transition from $n = 3$ into a chosen Rydberg state. The IR wavelength can be tuned from 1671 nm to 1715 nm.

By means of the excitation, the lifetime of Ps is greatly enhanced, see Eq. (2), increasing the distance the Ps* can travel in vacuum before annihilation (as well as the cross section for antihydrogen generation through charge exchange).

In the 1 T antihydrogen production region the Ps* experience an adverse effect that can cause ionisation, since they fly through a 1 T magnetic field at a set of velocities $\{v\}$ which are determined by the partial thermalisation with the Ps target. Traveling at velocity $\mathbf{v}$ a $n = 17$ Ps* 'quasi'-atom (we neglect fine and hyperfine splitting) experiences an electric field $\mathbf{E} = \mathbf{v} \times \mathbf{B}$ that has an ionising effect for velocities exceeding $\sim 170\ 000$m/s which corresponds to a temperature of about 2000K. In this classical estimate we assume a distance $\langle r \rangle$ of 32nm [32] between positron and electron and ionisation energy $|E_{io}| = |E_b - E_n|$, where E_b refers to the binding energy and E_n is the energy of the excited state. A non-orthogonal angle between velocity and B-field gives rise to much larger cut-off velocities and is infinite for $\mathbf{v} \parallel \mathbf{B}$.

For a more in-depth treatment of the laser system the reader may refer to [33] and references therein.

2.6. Pulsed antihydrogen production

The pulsed production of antihydrogen in the AE$\bar{g}$IS experimental scheme relies on charge exchange of Rydberg Ps and $\bar{p}$, see Eq. (1), where electron and antiproton 'swap' place. Once a fraction of the Rydberg positronium has entered the antihydrogen production trap through the perforated part of some of the electrodes, see Fig. 4, and reaches the vicinity of the stored antiprotons, charge exchange can happen.

The cross section for the reaction is proportional to the fourth power of the principal quantum number n

$$\sigma \propto a_0 n^4 \ , \tag{3}$$

where a_0 refers to the Bohr radius (~ 0.05nm) [34, 35]. The cross section is largest for a given principal quantum number n, when matching of the Ps velocity v_{Ps} and positron angular velocity v_{orb} occurs, i.e. $k = \frac{v_{Ps}}{v_{orb}} < 1$ [36, 37]. For $n = 17$ we expect a cross section of $\sigma \approx 10^{-10}\mathtt{cm}^2$ [37].

In this scheme of pulsed antihydrogen production the formed antihydrogen's temperature is largely determined by the antiproton temperature before the charge exchange. Since the quantum distribution of the Ps* is addressed by the wavelength and width of the IR laser it is narrow and well-determined and such is the resulting quantum distribution of the anticipated Rydberg antihydrogen.

The annihilation signals on the trap walls of freely-roaming, neutral $\bar{H}^*$ can be registered through coincidence counts in the signal of the digitised scintillator slabs.

3. Discussion

In this article we have given an overview of the experimental protocol leading up to pulsed antihydrogen formation through charge exchange. Experimental techniques from NNP physics, positron, positronium, laser and detector physics all contribute to the protocol. The proficiency lies in arranging and advancing the techniques in accordance to the experimental approach to testing the WEP with pulsed antihydrogen [34].

The initial steps in the experimental protocol are the simultaneous preparation of antiprotons and positrons. Antiprotons are caught, cooled, manipulated and finally transfered, stored and stacked in the antihydrogen production trap, see Section 2.2. Positrons are moderated, buffer-gas cooled and accumulated before their bunched injection into the main trap system (Section 2.3). The injection of the positron bunch into the nanochannelled target generates positronium, see Section 2.4, which partially thermalises with the nanopore walls of the material before the surviving Ps fraction is expelled into vacuum.

The preparation of Ps for antihydrogen generation through pulsed charge exchange is described in Section 2.5. Ortho-Ps is excited into a Rydberg state via a two-step excitation with a UV and IR laser pulse ($n = 1 \rightarrow n = 3$ and $n = 3 \rightarrow$ Rydberg state). The laser-excited quantum distribution of the Rydberg Ps* is very narrow.

The injection of the positron bunch and subsequent laser excitation are timed such that the scintillator slabs, see Section 2.1, start operating in analogue mode. They are ready to record candidates for antihydrogen production, the onset of which is possible once the Rydberg positronium enters the antihydrogen production trap where the antiproton plasma is stored.

In Section 2.6, the likelihood of an individual charge exchange process is illustrated which increases with the fourth power of the principal quantum number n, and for a given principal quantum number is most pronounced for a matching of Ps velocity and positron angular velocity [36, 37]. The global prospect of antihydrogen generation is proportional to the product of the absolute numbers of positrons/Ps* and $\bar{p}$ available from the ^{22}Na source/Ps target conversion and the antiproton decelerator at CERN. Of course, also geometrical factors of antiproton plasma size and incident Ps* angles determine the yield and the highest Ps* quantum numbers n_{max} that survive field ionisation.

The experimental protocol discussed here is complemented by a variety of protocols tailored to develop and explore the antiproton, positron, positronium and detector physics of the experiment. In the cyrogenic traps of the main apparatus electrons or combined electron antiproton plasmas are manipulated routinely [23]. So are positron plasmas in the positron system which can be operated independently from the rest of the apparatus and comprises a test chamber designed for this purpose, see Fig. 5. There is an extensive physics program going on for the positronium/laser physics [38, 39]. Adjacent to the AE$\bar{g}$IS antiproton beam line is the GRACE beam line which is used as an antiproton detector testing ground and can be operated at the same time as the protocol for pulsed antihydrogen production using antiproton bunches rejected by the main experiment.

4. Outlook

Since the antihydrogen production protocol is well-tested we are looking forward to pulsed antihydrogen generation and detection. As pointed out in Sections 2.4 and 3 the antihydrogen production rate through charge exchange is directly proportional to the number of $\bar{p}$s available. The Extra Low Energy Antiproton (ELENA) ring, which started its test phase in 2017, will provide AE$\bar{g}$IS and the other AD experiments with less energetic antiprotons at a higher rate from 2021 onwards, which will lead to a 100−fold increase in trappable antiprotons per bunch [40]. The higher numbers and higher repeatability promise higher overall antihydrogen yield.

In addition to the absolute antihydrogen numbers its temperature is of utmost importance for an eventual measurement of the gravitational acceleration $\bar{g}$. The temperature is, in the regime we are operating in, mostly determined by the antiproton temperature. Calculations show that it is feasible to use laser cooled anionic molecules as a sympathetic cooling source for antiprotons [41] – experimental developments and tests are on their way.

With a high yield of sub-Kelvin antihydrogen atoms, beam formation through Stark acceleration [20] and subsequent deexcitation of the antihydrogen Rydberg states will be combined with the gravity module [12].

5. Acknowledgements

We thank the members of the AE$\bar{g}$IS collaboration for illuminating discussions, in particular Michael Doser and Gemma Testera, and we are grateful for the invitation of the organizers of the symposium. Partial financial support by the German Federal Ministry of Education and Research is thankfully acknowledged.

References

[1] Doser M et al. 2012 Exploring the WEP with a pulsed cold beam of antihydrogen *Class. Quantum Grav.* **29**, 18

[2] Sakharov A D 1967 Violation of CP Invariance, C asymmetry, and baryon asymmetry of the universe *ZhETF Pis'ma* **5** 32

[3] Laurent C, Drewes M and Shaposhnikov M 2012 Matter and antimatter in the universe *New J. Phys.* **14** 095012

[4] Cohen A G, De Rújula A and Glashow S L 1998 A Matter-Antimatter Universe? *Astrophys. J.* **495** 539

[5] Hughes R J and Holzscheiter M H 1991 Constraints on the gravitational properties of antiprotons and positrons from cyclotron-frequency measurements *PRL* **66** 854

[6] Close F 2009 *Antimatter* (New York : Oxford University Press Inc.)

[7] Tietje I C 2018 Low-energy antimatter experiments at the antiproton decelerator at CERN: Testing CPT invariance and the WEP *J. Phys.: Conf. Ser.* **1071** 012021

[8] Aaij R et al. 2016 Search for Violations of Lorentz Invariance and CPT Symmetry in B_s^0 Mixing *PRL* **116** 241601

[9] Adam J et al. 2015 Precision measurement of the mass difference between light nuclei and anti-nuclei. *Nat. Phys.* **11**, 811

[10] Pérez P and Sacquin Y 2012 The GBAR experiment: gravitational behaviour of antihydrogen at rest *Class. Quantum Grav.* **29** 184008

[11] Hangst J S et al. 2016 *Addendum to the ALPHA Proposal; The ALPHA-g Apparatus* (CERN-SPSC-2016-031. SPSC-P-325-ADD-1)

[12] Aghion S et al. 2014 A moiré deflectometer for antimatter *Nat. Comm.* **5**, 4538

[13] Gligorova A 2014 *Development and Data Analysis of a Position Detector for AE$\bar{g}$IS (Antimatter Experiment: Gravity, Interferometry, Spectroscopy)* (University of Bergen)

[14] Dubin D H E and O'Neil T M 1999 Trapped nonneutral plasmas, liquids, and crystals (the thermal equilibrium states) *Rev. Mod. Phys.* **71** 87

[15] Surko C M 2010 *Accumulation, Storage and Manipulation of Large Numbers of Positrons in Traps I. – The Basics* **174** (Proc. of the International School of Physics "'Enrico Fermi" : Course CLXXIV)

[16] Aghion S et al. 2016 Laser excitation of the $n = 3$ level of positronium for antihydrogen production *Phys. Rev.* A **94** 012507

[17] Davidson R C 2001 *Physics of Nonneutral Plasmas* (Imperial College Press and World Scientific Publishing Co. Pte. Ltd.)

[18] Mariazzi S, Bettotti P, Larcheri S, Toniutti L and Brusa R S 2010 High positronium yield and emission into the vacuum from oxidized tunable nanochannels in silicon *Phys. Rev.* B **81** 235418
[19] Antiproton Decelerator website : https://espace.cern.ch/AD-site/default.aspx
[20] Vliegen E and Merkt F 2006 Stark deceleration of hydrogen atoms *Journ. of Phys.* B **39** 241
[21] Holmestad H 2018 *Data Analysis, Simulations, and Reconstruction of Antiproton Annihilations in a Silicon Pixel Detector* (University of Oslo)
[22] Zurlo N et al. 2020 Calibration and Equalisation of Plastic Scintillator Detectors for Antiproton Annihilation Identification Over Positron/Positronium Background *Acta Phys. Pol.* B **51** 213
[23] Aghion S et al. 2018 Compression of a mixed antiproton and electron non-neutral plasma to high densities *The European Physical Journal* D **72** 76
[24] Anderegg F 2015 *Rotating Wall Technique and Centrifugal Separation* (World Scientific Review Volume)
[25] Khatri R et al. 1990 Improvement of rare-gas solid moderators by using conical geometry *Appl. Phys. Lett.* **57**, 2374
[26] Rienäcker B 2015 *Investigation of positron/positronium converter targets at AEgIS (CERN)* (University of Applied Sciences Munich)
[27] Greaves R G and Surko C M 1996 Solid neon moderator for positron-trapping experiments *Canadian Journ. of Phys.* **74** 445
[28] Schultz P J and Lynn K G 1988 Interaction of positron beams with surfaces, thin films, and interfaces *Rev. Mod. Phys.* **60** 701
[29] Weng H M, Ling C C, Beling C D, Fung S, Cheung C K, Kwan P Y and Hui I P 2004 Tungsten mesh as positron transmission moderator in a monoenergetic positron beam *Nuclear Instr. and Meth. in Phys. Res.* B **225** 397
[30] Williams A I, Murtagh D J, Fayer S E, Andersen S L, Chevallier J, Kövér Á, Van Reeth P, Humberston J W and Laricchia G 2015 Moderation and diffusion of positrons in tungsten meshes and foils *J. Appl. Phys.* **118** 105302
[31] Surko C M Leventhal M, Passner A 1989 Positron Plasma in the Laboratory *Phys. Rev. Lett.* **62** 901
[32] Aghion S et al. 2016 Laser excitation of the $n = 3$ level of positronium for antihydrogen production *Phys. Rev.* A **94** 012507
[33] Yzombard P 2016 *Laser Cooling and Manipulation of Antimatter in the AEgIS Experiment* (Université Paris-Sarclay)
[34] Drobychev G et al. 2007 *Proposal for the AEgIS Experiment at the CERN antiproton decelerator* (CERN-SPSC-2007-017. SPSC-P-334)
[35] Charlton M 1990 Antihydrogen production in collisions of antiprotons with excited states of positronium *Phys. Lett.* A **143**, 143
[36] Massey H S W 1949 Collisions between atoms and molecules at ordinary temperatures *Reports on Progress in Physics* **12** 248
[37] Krasnický D, Caravita R, Canali C and Testera G 2016 Cross section for Rydberg antihydrogen production via charge exchange between Rydberg positroniums and antiprotons in a magnetic field *Phys. Rev.* A **94** 022714
[38] M Antonello et al. 2019 Efficient $2\,^3S$ positronium production by stimulated decay from the $3\,^3P$ level **100** 063414
[39] Amsler C et al. 2019 Velocity-selected production of $2\,^3$S metastable positronium *Phys. Rev.* A **99** 033405
[40] ELENA decelerator website: https://espace.cern.ch/elena-project/sitepages/home.aspx
[41] Gerber S, Fesel J, Doser M and Comparat D 2018 Photodetachment and Doppler laser cooling of anionic molecules *New Journ. of Phys.* **20** 023024